Fuel Processing Technology 278 (2025) 108327

Contents lists available at ScienceDirect

Fuel Processing Technology

journal homepage: www.elsevier.com/locate/fuproc

Thermal evolution and hydrocarbon generation of organic matter in shales via sequential high-pressure hydrous pyrolysis: Implications for in-situ conversion of unconventional resource

Fengtian Bai [a,b,c], Clement N. Uguna [c], Will Meredith [c], Colin E. Snape [c], Christopher H. Vane [d], Chenggong Sun [c,e,*]

[a] Key Laboratory of Geophysical Exploration Equipment, Ministry of Education, College of Construction Engineering, Jilin University, Changchun 130026, China
[b] State Key Laboratory of Deep Earth Exploration and Imaging, College of Construction Engineering, Jilin University, Changchun 130026, China
[c] Faculty of Engineering, University of Nottingham, Nottingham NG7 2TU, UK
[d] Organic Geochemistry Facility, British Geological Survey, Keyworth, Nottingham NG12 5GG, UK
[e] School of Chemical Engineering, University of Birmingham, Birmingham, B15 2TT, UK

ARTICLE INFO

Keywords:
Organic-rich shales
Sequential high-pressure hydrous pyrolysis
Hydrocarbon generation
Organic matter maturation
Biomarkers

ABSTRACT

Understanding kerogen transformation under geological conditions is critical for optimizing the in-situ conversion (ISC) process of organic-rich unconventional resources. Sequential high-pressure hydrous pyrolysis was employed to investigate the geological thermal evolution and hydrocarbon generation mechanisms of organic matter in immature Huadian (Type II_1 kerogen) and Fushun (Type I kerogen) shales. Experiments progressed through four thermal stages, that is Stage 1 (350 °C, 6 h), Stage 2 (350 °C, 24 h), Stage 3 (380 °C, 24 h), and Stage 4 (420 °C, 24 h), with comprehensive analysis of hydrocarbon products by gas-chromatography mass-spectrometry and solid residues by vitrinite reflectance (Ro) and Rock-Eval pyrolysis. The results revealed that the hydrocarbon-generation potential of these two shales declined sharply with a Ro of 0.78–1.23 %, correlating with peak oil generation. Type I kerogen (Fushun) exhibited higher reactivity, generating twice the cumulative oil yield (normalized by TOC) compared to Type II_1 (Huadian) and transitioning earlier to oil dominance. Biomarker evolution (OEP decline, sterane/hopane isomerization) in expelled oil and declining gas dryness index ($C_1/\Sigma C_1–C_5$) correlated strongly with the maturity of organic matter, enabling non-destructive ISC monitoring. Compared to typical temperatures used in ex-situ retorting (520 °C), the kerogen conversion was completed at lower temperatures of 350–420 °C in this study, validating prolonged heating as a viable low-energy ISC strategy. However, high-pressure conditions in geological formations may impede hydrocarbon expulsion efficiency, leading to the retention of viscous bitumen and thus necessitating engineered solutions for effective oil recovery. This research enriches the understanding of high-pressure pyrolysis mechanisms of immature/low-maturity unconventional resources and establishes a geochemical framework for optimizing ISC in recovering the oil from these source rocks, ultimately contributing to advancing sustainable exploitation of unconventional resources.

1. Introduction

In-situ conversion (ISC) technologies are essential for unlocking the vast potential of organic-rich shale resources, such as oil shale and low-maturity shale oil [1–5]. Oil shale, rich in solid organic matter (kerogen, vitrinite reflectance Ro < 0.5 %), requires subsurface heating to generate shale oil and gas, offering a major alternative to conventional petroleum [6,7]. Similarly, low-maturity shale oil resources, up to 25 % of liquid hydrocarbon maintaining in the shale (Ro = 0.5–1.0 %) and at least 40 % unconverted organic materials, also demand subsurface pyrolysis for economic recovery [5,8,9].

Prior studies highlight temperature, heating rate, and mineral composition as key controls on the oil yield and composition of shale oil from organic-rich shales, as well as on the pore evolution (porosity and permeability) of shales, a factor that is crucial for hydrocarbon migration underground [10–13]. While temperature is unequivocally the

* Corresponding author at: School of Chemical Engineering, University of Birmingham, Birmingham B15 2TT, UK.
E-mail address: c.sun.2@bham.ac.uk (C. Sun).

https://doi.org/10.1016/j.fuproc.2025.108327
Received 29 April 2025; Received in revised form 16 August 2025; Accepted 1 September 2025

primary driver of pyrolysis reactions, providing the necessary activation energy for bond cleavage, pressure exerts a significant secondary influence, shaping reaction kinetics, product distributions, and potentially reaction pathways [14–18]. Critically, kerogen decomposition under lithostatic pressure and confined pore fluids involves hydrocarbon expansion with pressure-dependent behaviour [19], which is highly relevant to the ISC process. Therefore, understanding the specific pyrolysis mechanisms under pressure conditions is essential for optimizing hydrocarbon yields from organic-rich shale resources through subsurface heating. Such pressure-dependent behaviour directly manifests in the modulation of both primary and secondary pyrolysis stages by pressure, exerting distinct effects on reaction pathways. For instance, elevated pressure inhibits the primary conversion of solid kerogen into volatile products while concurrently accelerating the secondary reactions of the pyrolyzates [15,17]. He et al. [20] investigated organic matter maturation in oil shale during high-pressure pyrolysis (8 MPa seepage pressure, 8 h isothermal heating), analysing residue properties (Ro and Rock-Eval T_{max}) to highlight the relationship between solid geochemical properties and organic matter thermal maturity. However, monitoring thermal maturity during the ISC process solely based on solid residue parameters (Ro, T_{max}) poses significant operational challenges in field applications. Building on this, subsequent work by He et al. [21] demonstrated that shale oil biomarkers undergo systematic structural and compositional changes that correlate strongly with the thermal maturity of the organic matter. These biomarker alterations provide reliable indicators of subsurface pyrolysis progression, enabling estimation of thermal maturity and conversion extent directly from produced oils, thus offering a practical method for monitoring and optimizing ISC processes.

Despite valuable insights, studies by He et al. [20,21] and others [14–18], which were conducted in anhydrous high-pressure systems, inadequately replicate the complexities of natural hydrostatically pressured, water-saturated environments typical of deep geological systems. This gap is particularly acute for low-maturity shale oil plays, which often reside at depths greater than 3–5 km where hydrostatic pressures exceed 30–50 MPa. In these systems, the presence of water can profoundly influence pyrolysis kinetics, reaction pathways, product yields, and hydrocarbon composition through mechanisms such as hydrolysis, dissolution, and phase behaviour. Consequently, additional studies incorporating more realistic conditions, including the presence of water and other formation fluids, are essential to fully elucidate the mechanisms and kinetics of petroleum generation and source rock maturation. Such knowledge is critical for guiding the development of more effective and efficient ISC technologies.

To address these limitations and bridge the knowledge gaps relevant to both oil shale and low-maturity shale oil exploitation, this study employs high-pressure hydrous pyrolysis experiments on immature Huadian (HD) and Fushun (FS) shales. Our aim is to investigate the thermal evolution of organic matter and hydrocarbon generation under simulated geological conditions. Experimental pressure was maintained at ~500 bar, corresponding to hydrostatic pressure at ~5 km depth based on a gradient of ~100 bars/km, thereby representing conditions typical for petroleum generation at such depths. Experimental temperatures (350–420 °C) were intentionally selected to exceed typical geothermal conditions at 5 km depth, which enables the acceleration of million-year natural maturation processes into a tractable 24-h experimental timeframe. Experiments comprised four sequential stages: Stage 1 (350 °C, 6 h), Stage 2 (350 °C, 24 h), Stage 3 (380 °C, 24 h), and Stage 4 (420 °C, 24 h). Following pyrolysis, the thermal evolution and hydrocarbon-generation potential of the organic matter were assessed through detailed characterisation of hydrocarbon gas and oil as well as solid residues. Additionally, the geochemical properties and characteristics of the generated hydrocarbons were thoroughly examined. Based on these analyses, hydrocarbon generation models were established for the two shales, and their implications for the ISC strategy are discussed. Critically, the experimental pressure design specifically mirrors the in-situ pressure regimes of deep low-maturity shale oil reservoirs, providing urgently needed data on kerogen transformation under geologically realistic hydrostatic conditions. Overall, this study advances the understanding of fundamental mechanisms underlying oil shale and low-maturity shale oil extraction, providing crucial insights to guide the design and optimization of future pilot-scale ISC experiments.

2. Materials and methods

2.1. Samples

The organic-rich oil shales investigated in this study were collected from the Huadian (HD) Basin and Fushun (FS) Basin in China (Fig. 1). The HD Basin, located on the northern flank of the Dunmi Fault Zone, is a semi-graben basin with an east-west orientation. Its oil shale deposits primarily derive from the Eocene HD Formation, and the specific samples used in this study obtained from the Gonglangtou area. In contrast, the FS Basin is situated at the western extremity of the Dunmi Fault Zone, a subsidiary structure of the major Tan Lu Fault Zone that extends northward. Classified as a residual basin within the Cenozoic rift system, the FS Basin contains oil shale deposits interbedded with coal seams. The FS shale samples analysed herein were sourced from an open-pit mine, where the oil shale and coal are mined concurrently. Prior to experiments, the raw (non-extracted) samples were mechanically crushed into 2–5 mm chips and homogenised to ensure uniformity.

2.2. High water-pressure pyrolysis experiments

Sequential pyrolysis experiments were conducted in a 25 ml Hastalloy cylindrical vessel under ~500 bar by sequential four stages: Stage 1 (350 °C, 6 h), Stage 2 (350 °C, 24 h), Stage 3 (380 °C, 24 h), and Stage 4 (420 °C, 24 h). This staged approach facilitated the evaluation of temperature-dependent hydrocarbon generation kinetics, source rock maturation effects, and the impact of supercritical water conditions (≥380 °C) on oil expulsion efficiency.

The experimental setup and core procedure were adapted from previous studies [19,22,23], with a schematic provided in Fig. 2. The experiment initiated with 25 g of shale samples. After each pyrolysis stage, the collected residual rocks were dried, with a portion reserved for subsequent analytical tests; the remaining residual shales were subjected to further pyrolysis at extended reaction times or elevated temperatures to assess non-cumulative hydrocarbon generation dynamics. Prior to each run, 20 ml of deionized water and a specified amount of shale were loaded into the pre-cleaned vessel. After assembly, the vessel

Fig. 1. Samples location map.

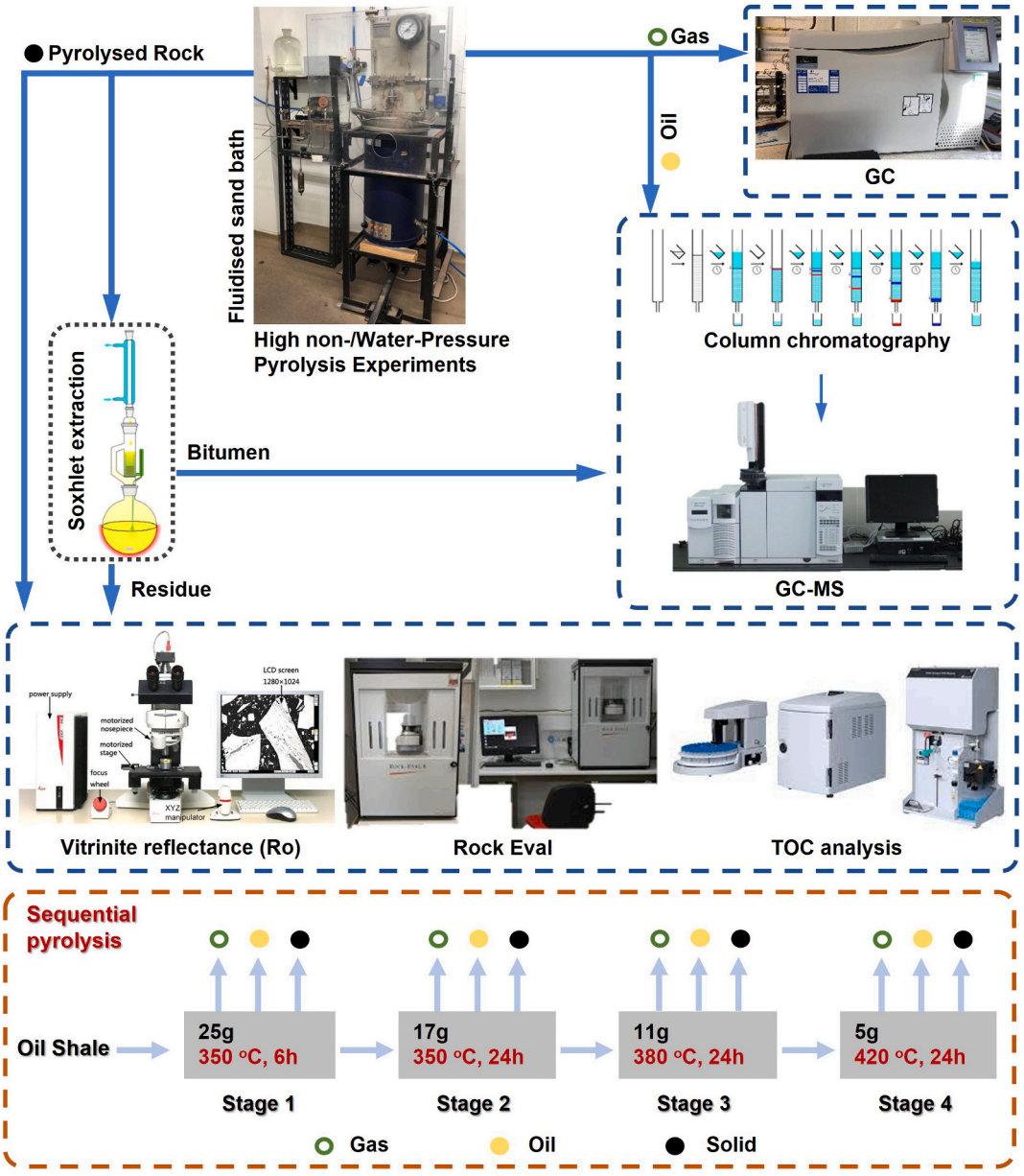

Fig. 2. Schematic diagram illustrating the temperatures, durations, and product analysis methods for the four stages of sequential pyrolysis experiments.

was purged with high-purity nitrogen (≥99.999 %) and pressurised to 2 bar to establish an inert atmosphere. Heating was achieved using a precisely controlled sand bath system preheated to the target temperature. Upon immersion and thermal equilibration, the internal pressure stabilized at a baseline value dependent on temperature and initial water fill. To achieve the target experimental pressure of ~500 bar, additional deionized water was injected into the vessel using an external compressed-air pump system. Overpressures (up to 605 bar) observed in some runs were attributed to thermal expansion of injected water and in-situ hydrocarbon gas generation.

After each pyrolysis run, the gaseous products were quantitatively collected using a gas-tight syringe for volume measurement. The gas composition (C_1–C_5 hydrocarbon) was immediately analysed by gas chromatography (Section 2.6). The expelled oil fraction, comprising free oil floating on top of the water and oil adhering to the vessel walls, was recovered by washing with cold dichloromethane (DCM). The remaining water phase was decanted, and the solid residue was oven-dried overnight at 45 °C.

For residue analysis, about 3 g of the dried rock was finely ground and subjected to Soxhlet extraction (Section 2.3) using a DCM/methanol mixture (93:7) to recover the solvent-extractable organic matter retained within the rock matrix, defined as “bitumen”. The extracted rock residue was retained for further characterisation. Asphaltene fractionation from the bitumen was performed only for Stages 1 and 2 by precipitation using DCM/heptane as solvent/non-solvent; insufficient yields precluded this separation for later stages. The maltene fraction (deasphalted bitumen) from bitumen of Stages 1–2, the whole bitumen from Stages 3–4, and the expelled oil were further separated into aliphatic hydrocarbons, aromatic hydrocarbons, and polar fractions using a silica-alumina gel column. The aliphatic hydrocarbon compositions were subsequently analysed by Gas Chromatography-Mass Spectrometry (GC–MS, Section 2.7). The remaining solid residues (without extraction) were subjected to the subsequent pyrolysis stage to assess non-cumulative hydrocarbon-generation potential.

2.3. Soxhlet extraction and bitumen quantification

Bitumen content in the initial and pyrolysed rock samples was

determined via exhaustive Soxhlet extraction. Approximately 3 g of finely ground rock powder (<200 mesh) was loaded into a pre-cleaned cellulose extraction thimble (pre-extracted with DCM/methanol (93:7) to remove impurities). Extraction was performed for >48 h using 150 ml of DCM/methanol mixture (93:7) in a 250 ml round-bottom flask. After extraction, the extracted rock was stored for subsequent analysis, and the bitumen-containing solvent was evaporated using a rotary evaporator until most of the solvent was removed. The residual bitumen was transferred to a pre-weighed vial using DCM and left to dry. The weight of the vial and extract was taken, and the bitumen weight was calculated by the difference after all the DCM had evaporated.

2.4. Vitrinite reflectance (Ro)

Vitrinite reflectance (Ro) was obtained on the initial (non-extracted) and solvent extracted residues of pyrolysed rocks. Samples were embedded in epoxy resin mounts and polished sequentially using silicon carbide papers to produce a scratch free polish surface. Measurements were made using a J&M TIDAS MSP 200 microscope in non-polarized light at a wavelength of 546 nm in oil immersion following the Chinese standard SY/T 5124–2012.

2.5. Rock-Eval pyrolysis and total organic carbon (TOC)

Rock-Eval pyrolysis and TOC determination were conducted on both initial and pyrolysed rocks, including non-extracted and solvent-extracted residues, using a Vinci Technologies Rock-Eval 6 standard instrument. About 60 mg of crushed powdered rock was heated in an N_2 atmosphere using an initial oven programme of 300 °C for 3 min and then from 300 to 650 °C at the rate of 25 °C min^{-1}. The oxidation stage was achieved by heating at 300 °C for 1 min and then from 300 to 850 °C at 20 °C min^{-1} and held at 850 °C for 5 min. Hydrocarbons released during the two-stage pyrolysis were measured using a flame ionization detector (FID), and CO and CO_2 were measured using an infrared (IR) cell [24].

2.6. Gas chromatography (GC) analysis

A Clarus 580 GC fitted with an FID and TCD detectors was used to analyse the gaseous products. 5 ml of gas samples was injected (split ratio 10:1) at 250 °C with separation performed on an Rt-Alumina Bond/KCl Plot fused silica 30 m × 0.32 mm × 5 μm column, with helium as the carrier gas. The oven temperature was programmed from 60 °C (13 min hold) to 180 °C (10 min hold) at 10 °C min^{-1}. Individual gas yields were determined quantitatively in relation to a separately injected C_1–C_5 mixture as an external gas standard. The total yield of the hydrocarbon gases generated was calculated using the total volume of generated gases collected in relation to the aliquot volume of gases introduced to the GC, using relative response factors of individual C_1–C_5 gases from a standard mixture of C_1–C_5 gases.

2.7. Gas chromatography–mass spectrometry (GC–MS) analysis

The aliphatic hydrocarbons of oil and bitumen from each stage were analysed by an Agilent GC–MS (7890B GC; 5977 A-mass selective detector (MSD)) in full scan mode (*m/z* 40–400) in 10 times split mode. Separation was achieved on an HP-5MS column (30 m × 0.25 mm i.d., 0.25 μm thickness) with Helium as the carrier gas, and an oven programme of 50 °C (hold for 2 min) to 300 °C (hold for 20.5 min) at 4 °C min^{-1}. Identification of individual compounds was performed by comparing experimental mass spectra with those in the NIST 14 Mass Spectral library and published data.

3. Results and discussion

3.1. Bulk geochemical parameters of initial samples

The Rock-Eval, TOC, and Ro results of the initial HD and FS oil shales are shown in Table 1. Both source rocks exhibit low thermal maturity, evidenced by same T_{max} of 436 °C and mean Ro of 0.42 % (HD) and 0.38 % (FS). The HD shale is rich in organic matter, with a TOC of 27.98 %, approximately three times higher than the FS shale (TOC = 8.79 %). Consistent with its low maturity, the initial HD shale shows a low free hydrocarbon yield (S_1 = 0.44 mg/g) and a high pyrolysable hydrocarbon potential (S_2 = 175.58 mg/g). The FS shale displays a slightly higher S_1 (0.91 mg/g) but a significantly lower S_2 (57.71 mg/g) than HD. Hydrogen index (HI) values confirm both samples are oil-prone (HD: 628 mg HC g^{-1} TOC $^{-1}$; FS: 657 mg HC g^{-1} TOC $^{-1}$). Cross-plots of HI vs. T_{max} and S_2 vs. TOC (Fig. S1) classify the HD kerogen as Type II_1 and FS kerogen as Type I. Moreover, S_2 vs. TOC and TOC vs. bitumen plots underscore the substantial hydrocarbon-generation potential of both shales (Fig. S2).

Soxhlet extraction yields (Table S2) reveal low initial bitumen contents in HD shale (0.57 %) and FS shale (0.75 %). Fractionation indicates low proportions of aliphatic (13.10 %) and aromatic (4.15 %) hydrocarbons in HD bitumen, while FS bitumen contains higher aliphatic (24.41 %) and aromatic (10.49 %) components.

The total ion current (TIC) chromatograms and *m/z* 191, m/z 217 chromatograms of the aliphatic fractions are shown in Figs. S3 and S4, and corresponding biomarker analysis are presented in Table 2, providing insights into organic matter source and maturity. As shown in Figs. S3 and S4, both shales display unimodal *n*-alkanes ranging from nC_{14} to nC_{39} with a maximum at C_{27} and significant odd-to-even predominance pattern at high molecular weights, indicative of substantial terrigenous plant input [25,26]. The higher Carbon Preference Index (CPI, 3.88) and Odd-to-Even Predominance Index (OEP, 4.50) in HD versus FS (1.76 and 1.89, respectively) confirm HD has a lower relative maturity [25,27]. The pristane/phytane (Pr/Ph) ratio of D shale (2.6), together with the results of the Pr/nC_{17} vs. Ph/nC_{18} cross-plot (Fig. S5), suggests terrigenous input under a predominantly oxidising environment for HD. In contrast, for FS shale, both the Pr/Ph ratio and Pr/nC_{17} vs. Ph/nC_{18} cross-plot indicate a depositional environment transitioning from transitional to oxidising conditions.

Significant different exist in hopanoid distributions of the aliphatic hydrocarbons fraction of HD and FS bitumens. The HD shale is characterized by abundant terpenes and ββ-hopanes, with C_{29} neoHop-13(18)-ene as the predominant hopanoid (Fig. S3). The presence of these labile compounds signifies very shallow diagenesis and minimal subsurface thermal alteration. In contrast, the FS hopanoid assemblage (Fig. S4) comprises mature 17α, 21β and 17β, 21α hopanes ranging from C_{27} to C_{34}, with the exception of C_{28} hopane. This assemblage is dominated by 17α, 21β C_{30} hopane, and homohopanes show a gradual decreasing trend in abundance ($C_{31} > C_{32} > C_{33} > C_{34}$). Key maturity indicators consistently confirm the low maturity of both HD and FS shale, with HD exhibiting a lower maturity level. Specifically, HD is characterised by a lower of C_{27} 17α(H)-22,29,30-trisnorhopane (Tm) to C_{27} 18α(H)-22,29,30-trisnorneohopane (Ts) ratio (Ts/(Ts + Tm), <0.3), a higher abundance of immature C_{27} 17β(H)-22,29,30-trinorhopane (βTm), significantly higher C_{29} and C_{30} βα/αβ hopane ratios (0.86 and 5.44 for HD, respectively, compared to lower values for FS), and lower C_{31} and C_{32} 22S/(22S + 22R) homohopane ratios (0.12 and 0.23 for HD versus 0.47 and 0.44 for FS). The higher 22S/(22S + 22R) ratios in FS than in HD suggest preferential microbial biodegradation of the 22R epimer in FS [28]. The presence of gammacerane in FS (Fig. S4) points to hypersaline depositional conditions [25,29,30], a biomarker that is absent in HD.

Sterane distributions are widely recognized as effective source discriminants. As shown in Fig. S3, HD steranes are dominated by regular C_{29}, C_{28} and C_{27} steranes (with a distribution pattern of $C_{29} > C_{28} > C_{27}$)

Table 1
Rock-Eval, TOC, and Ro of the initial shales, extracted and unextracted residues from high-pressure hydrous pyrolysis.

Samples	Experiment		S_1 (mg/g)	S_2 (mg/g)	T_{max} (°C)	TOC (%)	HI (mg HC g^{-1} TOC $^{-1}$)	Ro (%)
HD	Initial		0.44	175.58	436	27.98	628	0.42 [30] [a]
	Stage 1	PR	17.28	139.82	447	25.30	553	
		Residue	0.29	96.00	446	18.92	507	0.78 [25]
	Stage 2	PR	41.70	128.16	440	26.94	476	
		Residue	0.23	50.16	447	15.99	314	0.82 [22]
	Stage 3	PR	40.52	59.85	443	22.01	272	
		Residue	0.10	14.08	451	15.06	93	1.23 [20]
	Stage 4	PR	2.53	5.59	578	14.43	39	
		Residue	0.05	2.42	585	13.92	17	1.99 [25]
FS	Initial		0.91	57.71	436	8.79	657	0.38 [20]
	Stage 1	PR	4.42	47.99	444	8.50	565	
		Residue	0.04	26.30	444	5.76	457	0.58 [20]
	Stage 2	PR	5.85	29.23	445	7.12	411	
		Residue	0.03	9.09	446	4.50	202	0.82 [18]
	Stage 3	PR	0.61	4.56	449	4.71	97	
		Residue	0.01	1.75	456	4.11	43	1.37 [16]
	Stage 4	PR	0.12	0.47	590	3.89	12	
		Residue	0.02	0.40	591	3.77	11	1.84 [12]

Notes: S_1: free hydrocarbons; S_2: hydrocarbons generated during Rock-Eval pyrolysis; T_{max}: temperature of maximum hydrocarbon generation; TOC: total organic carbon; HI: hydrogen index; PR: Solid residue pre-extraction; Residue: Solid residue post-extraction; [a] the number of vitrinite particles measured in bracket.

Table 2
Biomarker analysis data of bitumen from both initial and pyrolysed HD and FS shales.

Sample	Experiment	CPI	OEP	Pr/Ph	Pr/C_{17}	Ph/C_{18}	m/z 191					m/z 217	
							Ts/(Ts + Tm)	C_{29} βα/αβ	C_{30} βα/αβ	C_{31} 22S/(22S + 22R)	C_{32} 22S/(22S + 22R)	C_{29} ααα 20S/(20S + 20R)	C_{29} αββ/(ααα + αββ)
HD	Initial	3.88	4.50	2.60	0.99	0.31	0.20	0.86	5.44	0.12	0.23	0.04	0.04
	Stage 1	1.36	1.44	5.08	1.05	0.17	0.03	0.73	0.98	0.39	0.38	0.25	
	Stage 2	1.22	1.28	4.55	0.22	0.04	0.04	0.48	0.76	0.52	0.54	0.49	
	Stage 3	1.16	1.21	2.55	0.04	0.01	0.12	0.24	0.63	0.58	–	–	
FS	Initial	1.76	1.89	1.51	2.90	2.01	0.28	0.28	0.16	0.47	0.44	0.16	0.25
	Stage 1	1.22	1.24	2.34	1.00	0.43	0.15	0.36	0.35	0.46	0.37	0.19	
	Stage 2	1.10	1.09	1.80	0.25	0.13	0.14	0.33	0.39	0.54	0.48	0.45	
	Stage 3	1.05	1.02	0.96	0.05	0.05	0.22	0.32	0.34	0.49	0.44	0.29	

Notes: CPI = $2 \times (nC_{23} + nC_{25} + nC_{27} + nC_{29} + nC_{31})/(nC_{22} + 2 \times nC_{24} + 2 \times nC_{26} + 2 \times nC_{28} + 2 \times nC_{30} + nC_{32})$alkanes; OEP = $1/4 \times (nC_{25} + nC_{27} + nC_{29})/(nC_{26} + nC_{28})$; αβ and βα (*m/z* 191) denote 17α(H)-hopanes and 17β(H)-moretanes, respectively; Ts = C_{27} 18α(H)-22,29,30-trisnorneohopane, Tm═C_{27} 17α(H)-22,29,30-trisnorhopane; βTm = C_{27} 17β(H)-22,29,30-trisnorhopane; βα, αβ, ααα and αββ (*m/z* 217) denote 13β(H),17α(H)-diasteranes, 13α(H),17β(H)-diasteranes, 5α(H),14α(H),17α(H)-steranes and 5α(H),14β(H),17β(H)-steranes, respectively.

and C_{29} diasteranes, with minimal pregnanes (C_{21}, C_{22}), consistent with significant land plant input. In contrast, FS exhibits a "V"-shaped distribution of regular steranes ($C_{29} \approx C_{27} > C_{28}$, Fig. S4), suggesting mixed terrigenous and algal sources, since C_{27} sterols are typically algal and C_{29} sterols are terrigenous [31–33]. The ternary plot of C_{27}, C_{28}, and C_{29} regular steranes (Fig. S6) confirms mixed land plant/planktonic organic matter for HD and FS shales, with a stronger terrigenous signal in HD. Crucially, the C_{29} ααα 20S/(20S + 20R) and C_{29} αββ/(ααα + αββ) sterane

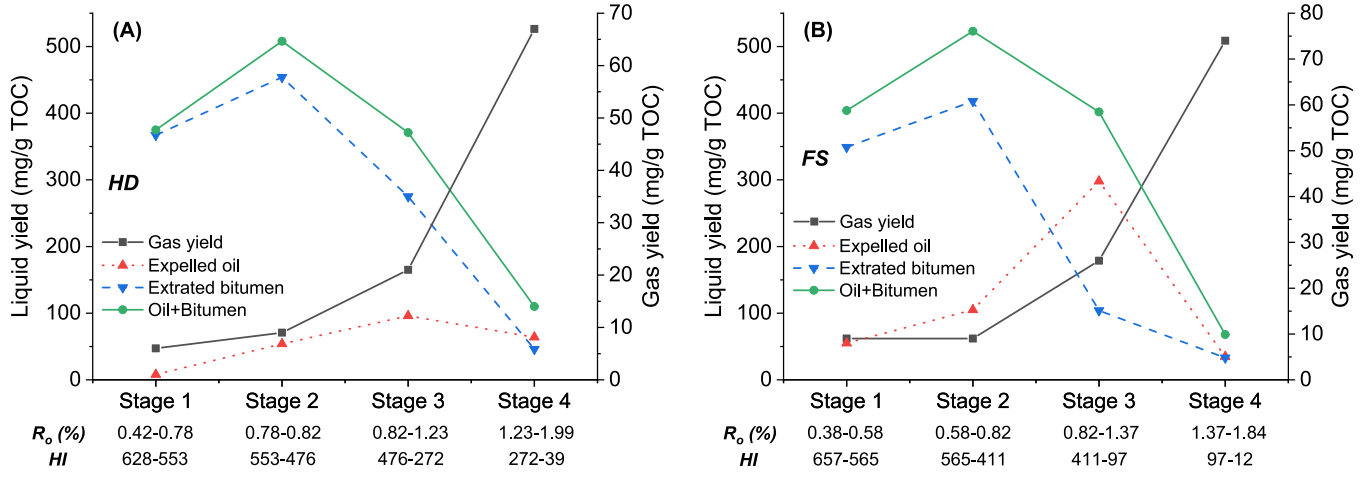

Fig. 3. Yields of total hydrocarbon gas (C_1-C_5), expelled oil, and retained bitumen (normalized to mg/g TOC of the rock at the start of each run) from sequential high-pressure hydrous pyrolysis experiments. (A) HD shale. (B) FS shale. The Ro and HI values shown beneath each histogram correspond to the start and end of each stage, respectively.

ratios for HD are 0.04 and 0.04, respectively, and for FS are 0.16 and 0.25 (Table 2), which are significantly below equilibrium values, unequivocally confirming that both shales were in an immature state prior to the oil generation window.

In summary, geochemical characterisation identifies the HD oil shale as containing immature Type II_1 kerogen with strong terrigenous input, while the FS shale contains immature Type I kerogen with mixed terrigenous and algal input. Both samples possess significant hydrocarbon-generation potential.

3.2. The evolution of hydrocarbon generation and maturation of organic matter under high-pressure water pyrolysis

3.2.1. Yields and composition of gas, expelled oil, and retained bitumen

Fig. 3 and Table S1 present hydrocarbon yields of HD and FS shales during each run. Total hydrocarbon gas (C_1–C_5) yields normalized to TOC show a progressive increase across stages for both shales, with significant escalation during Stages 3 and 4. Specifically, gas yields of HD increased from 6 mg/g TOC (Stage 1) to 64 mg/g TOC (Stage 4), which from 9 mg/g TOC (Stage 1) to 114 mg/g TOC (Stage 4) of FS. And the gas yields of FS shale were slightly higher than that of HD except in Stage 2. The generated hydrocarbon gases from HD and FS were mainly alkanes, especially methane, ethane, and propane. As shown in Table S1, Methane dominated the gas composition, increasing steadily in HD from 2.9 mg/g TOC of Stage 1 to 18.9 mg/g TOC of Stage 4. Methane in FS stayed consistent in the first two stages while a notable increase was observed in Stages 3 and 4. The dryness index ($C_1/\Sigma C_1$–C_5, Table S1) decreased for HD, particularly in Stage 4. FS exhibited a comparatively stable dryness index across Stages 1–3 (36–38 %), with only a slight increase in Stage 3, before decreasing to 29 % in Stage 4, which is comparable to that of HD in Stage 4. The declining dryness indicates an increasing contribution from secondary cracking of liquid hydrocarbons to the gas phase, not primary kerogen degradation [34,35].

Expelled oil and retained bitumen (solvent-extractable) yields (Fig. 3, Table S1) followed a characteristic pattern that initially increased and reached a peak at Stage 2 of bitumen and Stage 3 of oil, followed by a decline. Bitumen yields consistently exceeded oil yields. The subsequent decrease in bitumen concurrent with peak oil expulsion in Stage 3 underscored its role as an intermediate product in kerogen conversion. Bitumen retention is thus governed by both generation from kerogen and expulsion efficiency. FS generated twice the cumulative oil yield (normalized by TOC) and superior oil expulsion efficiency compared to HD (Table S1), reflecting the higher reactivity and oil-prone nature of its Type I kerogen. The decline in liquid yields by Stage 4 resulted from the progressive depletion of the hydrocarbon-generation potential of shales during preceding stages.

Ternary plots of expelled oil and bitumen composition of both HD and FS samples (Fig. S7) reveal a systematic evolution which the proportion of polar fraction decreased from Stage 1 to Stage 3, while aliphatics increased, indicating progressive thermal upgrading of both retained and expelled hydrocarbons. Stage 4 data were excluded due to the sampling limitations and excessive light hydrocarbon loss.

3.2.2. Thermal maturation and hydrocarbon-generation potential of pyrolysed rock

The Ro, TOC, and Rock-Eval pyrolysis data of the pyrolysed rock were investigated to reveal the thermal evolution and hydrocarbon-generation potential of organic matter during pyrolysis, with the results presented in Table 1. The mean Ro of the HD shale increased from an initial value of 0.42 % to 1.99 % at Stage 4, while the FS sample followed a similar pattern, rising from 0.38 % (initial) to 1.84 % (Stage 4). This confirms significant maturation, transitioning through the oil window to a high/over-maturity stage. TOC analysis (Table 1) showed a decreasing trend for both extracted and unextracted residues, except for the HD at Stage 2, which is attributed to hydrocarbon generation/expulsion. The lower TOC of extracted residues compared to unextracted values is due to the bitumen removal. Overall, 50 % (HD) and 57 % (FS) of the initial organic matter was converted to oil and gas during the high-pressure pyrolysis process.

The S_1 parameter (free hydrocarbons) initially increased and peaked at 41.7 mg/g (HD) and 5.85 mg/g (FS) in Stage 2 for unextracted residue, but became negligible after extraction, confirming free hydrocarbons primarily originate from retained bitumen. The kerogen-bound hydrocarbons (S_2) declined continuously in both extracted and unextracted residues (Table 1), and the TOC vs. S_2 cross-plot of unextracted pyrolysed rock (Fig. 4) exhibited a positive correlation, reflecting the progressive conversion of kerogen and depletion of hydrocarbon-generation potential. The unextracted residues of HD shale still showed excellent oil potential even after Stage 3 (Fig. 4). In contrast, the hydrocarbon-generation potential of FS declined more rapidly than that of HD, consistent with its higher reactivity, and the residue from Stage 4 of FS exhibited poor hydrocarbon-generation potential (Fig. 4).

Similar decreasing trends were observed in HI of both extracted and unextracted residues, highlighting the decreasing hydrocarbon-generation potential of HD and FS shales. For unextracted residue, HI values dropped below 100 mg/g TOC by Stage 4 of HD and by Stage 3 of FS, indicating very poor hydrocarbon-generation potential. The T_{max} values of residues from HD and FS (Table 1, Fig. S8) remained stable between 440 and 449 °C (unextracted residues) and 444–451 °C (extracted residues) across Stages 1–3, consistent with the oil window (mature stage), but increased sharply to 578–591 °C in Stage 4, confirming entry into the gas window (high/over-maturity), which aligns with Ro data.

3.2.3. Lipid biomarker assemblages

(1) Retained bitumen

Fig. 5 and Fig. 6 present the *m/z* 71, m/z 191, and m/z 217 chromatograms of retained bitumen from the sequential pyrolysis for HD and FS shales, respectively, and the corresponding biomarker ratios are listed in Table 2. Data from Stage 4 were excluded to avoid potential inaccuracies or unreliability arising from insufficiently collected sample.

As presented in Fig. 5A, the *n*-alkane distribution of HD bitumen evolved from a bimodal pattern (Stages 1–3) with high molecular weights and a strong odd-to-even predominance, to a unimodal distribution in Stage 4, dominated by short/medium-chain *n*-alkanes with no odd-to-even predominance, indicating increased maturity of the organic matter. For FS bitumen, a unimodal *n*-alkane distribution was observed across Stages 1–3 (Fig. 6A), with a slight shift from high molecular

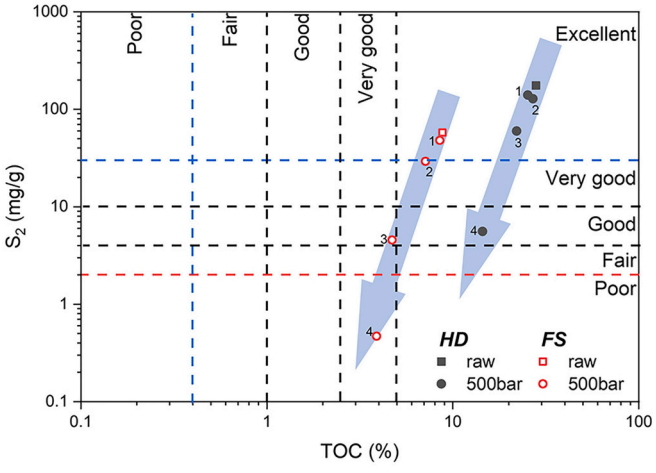

Fig. 4. Cross-plot of the TOC vs. S_2 showing the hydrocarbon-generation potential of unextracted initial and solid residue (1, 2, 3, and 4 refer to the Stage 1, Stage 2, Stage 3, and Stage 4, respectively).

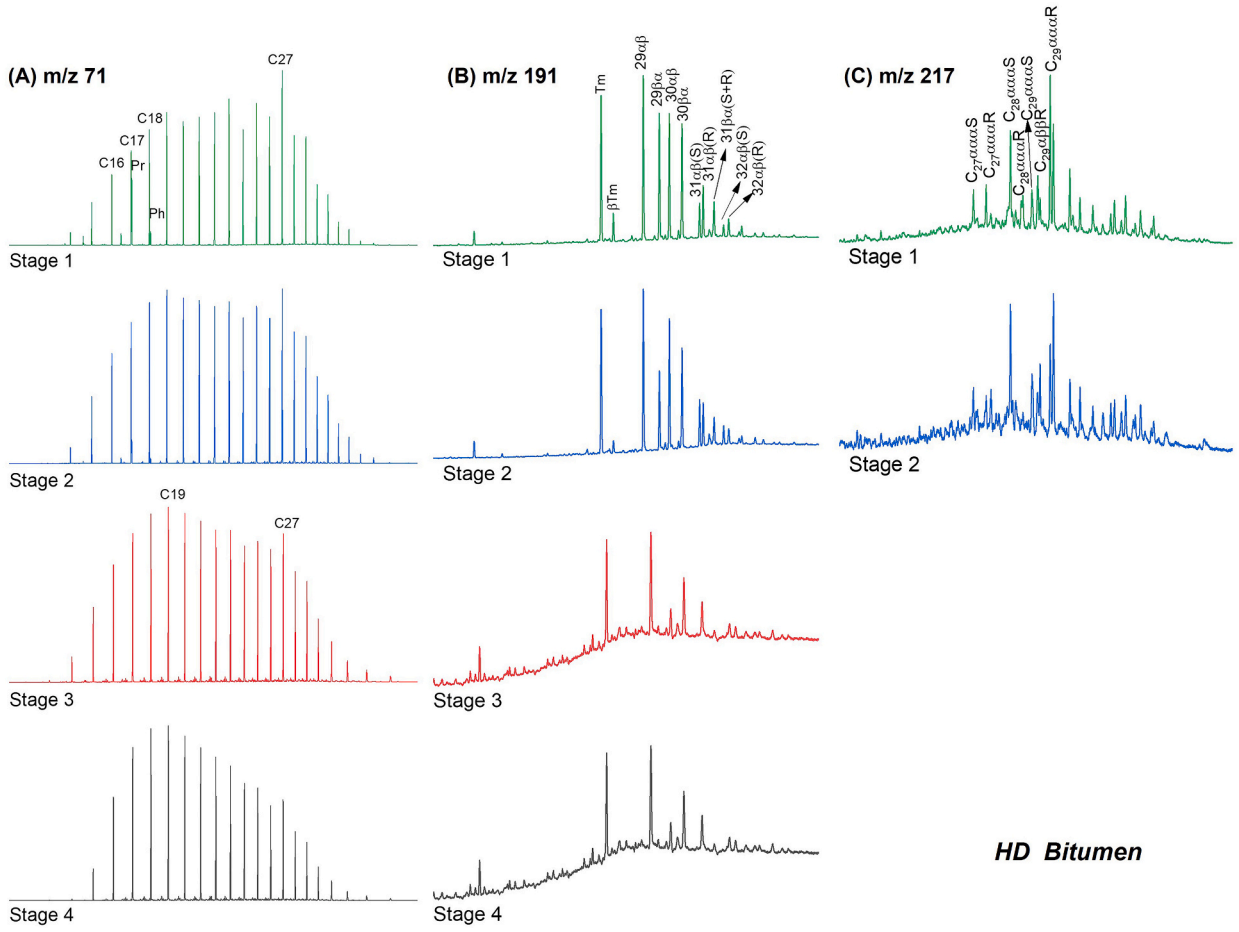

Fig. 5. Partial *m/z* 71, m/z 191, and m/z 217 mass chromatograms of the aliphatic hydrocarbon fraction in retained bitumen from each stage of HD samples.

weights to low molecular weights, but weak odd-to-even predominance pattern was only detected in Stage 1. As shown in Table 2, the CPI and OEP values for bitumen in both HD and FS decreased progressively, stabilising around 1.0 (equilibrium) by Stage 3. Specifically, the values for HD shale were 1.16 and 1.21, respectively, while those for FS shale were 1.05 and 1.02, respectively. The shift in the *n*-alkanes maximum peak and the gradual weakening of odd-to-even predominance in both HD and FS samples further reflect increasing organic matter maturity during thermal evolution. Additionally, FS consistently exhibited lower CPI/OEP values than HD at equivalent stages, confirming its relatively higher maturity.

Isoprenoids are more stable than *n*-alkanes and can be largely retained during thermal degradation. As shown in Table 2, the Pr/Ph ratio of bitumen from HD and FS samples displayed a consistent pattern showing an initial increase in Stage 1 followed by a decrease in subsequent stages, reflecting the completion of processes in kerogen decomposition. Pristane precursors can be preferentially released from kerogen compared to phytane precursors [36]. The inherently higher abundance of pristane precursors in kerogen [37] and the dominant demethylation process of phytane to pristane collectively drive the early increase in Pr/Ph ratio observed at Stage 1. The subsequent decline in ratios from Stage 2 onward stemmed from the delayed liberation of phytane precursors, which persist into higher maturity stages [38], progressively enriching the hydrocarbon phase in phytane. Furthermore, FS generally exhibited lower Pr/Ph ratios than HD samples at equivalent maturity stages (Table 2). This difference arises from the reduced release of phytane precursors in HD, as corroborated by the lower phytane peaks in HD *m/z* 71 chromatograms (Figs. 5 and 6). The Pr/nC_{17} and Ph/nC_{18} ratios consistently decreased from Stage 1 to Stage 3 (Table 3), indicating a declining relative abundance of isoprenoids compared to *n*-alkanes with increasing maturity.

Compared to the initial HD shale (Fig. S3), the concentrations of unstable terpenes and ββ hopanes in HD samples decreased, while the content of stable αβ hopanes increased as thermal evolution progressed from Stage 1 to Stage 4 (Fig. 5B). As shown in Table 2, for HD bitumen, during thermal evolution from the initial shale to Stage 3, the Ts/(Ts + Tm) ratio first decreased to 0.030–0.04 in Stages 1–2, followed by an increase in Stage 3; the C_{29} βα/αβ and C_{30} βα/αβ ratios decreased progressively; and the C_{31} 22S/(22S + 22R) and C_{32} 22S/(22S + 22R) ratios increased and stabilized within the equilibrium range of 0.54–0.58. These systematic biomarker evolutions in the HD sample across Stages 1–3 confirm progressive thermal maturation of their organic matter [39,40]. A similar trend is evident in the Ts/(Ts + Tm) ratio of the FS sample, which first decreased to 0.15 and 0.14 at Stage 1 and Stage 2, respectively, before increasing to 0.22 in Stage 3. In contrast, the C_{29} βα/αβ and C_{30} βα/αβ ratios in FS samples remained relatively constant at 0.3–0.4, while the C_{31} 22S/(22S + 22R) and C_{32} 22S/(22S + 22R) ratios were maintained between 0.44 and 0.54. These stable patterns reflect the limited utility of these ratios as a maturity indicator.

As thermal evolution progressed, the C_{29}ααα sterane 20S/(20S + 20R) ratio of HD bitumen increased from 0.04 (initial) to 0.49 (Stage 2), reaching its equilibrium, as observed in Table 2. FS bitumen exhibited a comparable pattern in the C_{29} ααα 20S/(20S + 20R) ratio, which increased from an initial value of 0.16 to 0.45 in Stage 2 before decreasing to 0.29 in Stage 3. This upward trend is attributed to the transformation of C_{29} ααα 20R sterane into C_{29} ααα 20S sterane, confirming a significant increase in maturity [21]. The decrease observed in Stage 3 of FS results from the preferential thermal alteration of the 20S

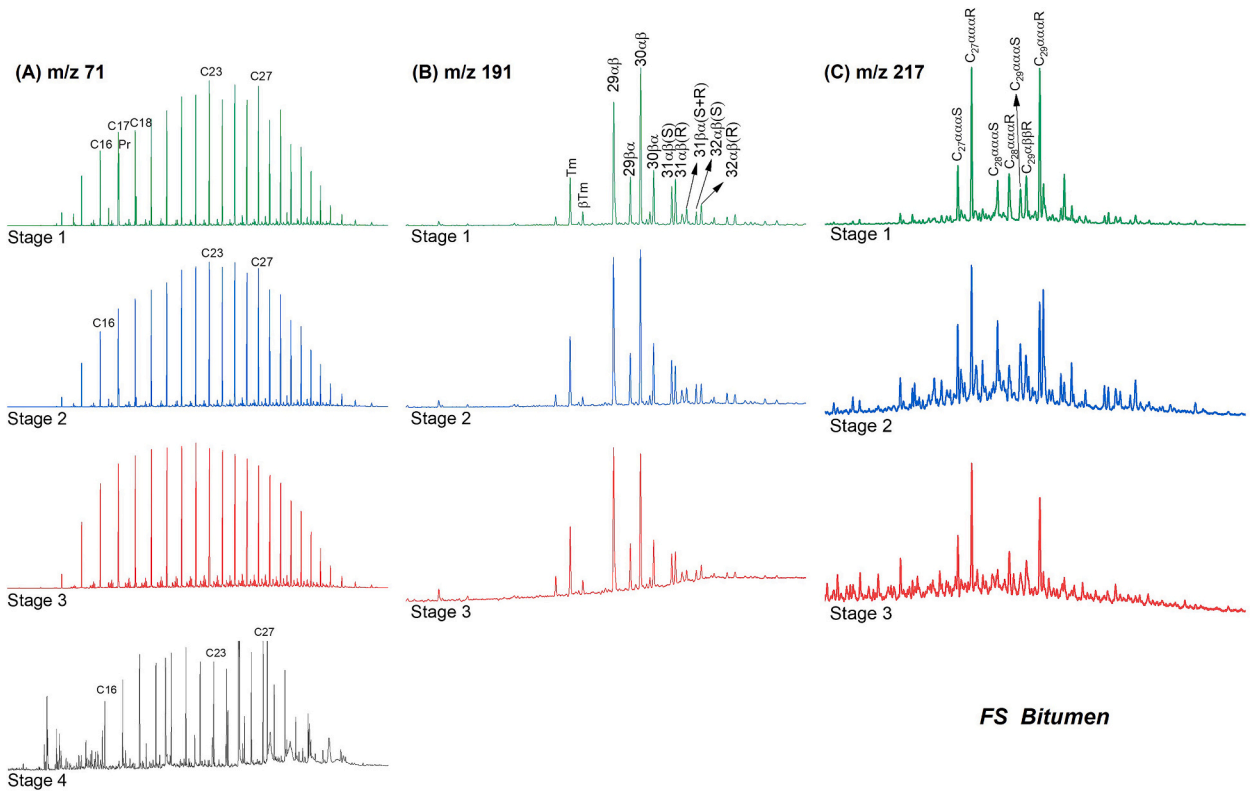

Fig. 6. Partial m/z 71, m/z 191, and m/z 217 mass chromatograms of the aliphatic hydrocarbon fraction in retained bitumen from each stage of FS samples. The m/z 71 mass chromatogram of Stage 4 corresponds to unfractionated bitumen due to insufficient samples.

Table 3
Biomarker analysis data of expelled oil of each stage.

Sample	Experiment	CPI	OEP	Pr/Ph	Pr/C_{17}	Ph/C_{18}	m/z 191					m/z 217
							Ts/(Ts + Tm)	C_{29} βα/αβ	C_{30} βα/αβ	C_{31} 22S/(22S + 22R)	C_{32} 22S/(22S + 22R)	C_{29}ααα 20S/(20S + 20R)
HD	Stage 1	2.07	2.38	1.99	1.01	0.23	0.19	0.53	0.80	0.44	0.48	0.31
	Stage 2	1.31	1.37	3.24	0.62	0.15	0.08	0.54	0.68	0.49	0.49	0.43
	Stage 3	1.18	1.22	2.69	0.08	0.03	0.12	0.33	0.53	0.56	0.53	–
FS	Stage 1	1.42	1.44	2.19	1.35	0.75	0.20	0.31	0.26	0.47	0.39	0.21
	Stage 2	1.19	1.17	2.27	0.62	0.31	0.16	0.32	0.34	0.49	0.42	0.26
	Stage 3	1.07	1.05	1.50	0.09	0.06	0.20	0.30	0.36	0.56	0.51	0.54

Notes: CPI = 2 × ($nC_{23} + nC_{25} + nC_{27} + nC_{29} + nC_{31}$)/($nC_{22} + 2 \times nC_{24} + 2 \times nC_{26} + 2 \times nC_{28} + 2 \times nC_{30} + nC_{32}$)alkanes; OEP = 1/4 × ($nC_{25} + nC_{27} + nC_{29}$)/($nC_{26} + nC_{28}$); αβ and βα (m/z 191) denote 17α(H)-hopanes and 17β(H)-moretanes, respectively; Ts = C_{27} 18α(H)-22,29,30-trisnorneohopane, Tm = C_{27} 17α(H)-22,29,30-trisnorhopane; βTm = C_{27} 17β(H)-22,29,30-trisnorhopane; βα, αβ, ααα and αββ (*m/z* 217) denote 13β(H),17α(H)-diasteranes, 13α(H),17β(H)-diasteranes, 5α(H),14α(H),17α(H)-steranes and 5α(H),14β(H),17β(H)-steranes, respectively.

isomer at very high maturity following equilibrium [41,42]. C_{29} ααα steranes became undetectable in HD Stages 3–4 and FS Stage 4, limiting the utility of this ratio beyond the peak oil generation window. These differences in biomarker characteristics are derived from distinct depositional environments between the HD and FS shales.

(2) Expelled oil

Figs. 7 and 8 present the *m/z* 71, m/z 191, and m/z 217 mass chromatograms of expelled oil from different thermal evolution stages of HD and FS samples, respectively, and corresponding biomarker data (Stage 4 data excluded) are shown in Table 3.

As illustrated in Fig. 7A, the *n*-alkane in HD expelled oil evolved from a unimodal distribution pattern (nC_{16} to nC_{33}) in Stage 1 with a pronounced odd-to-even carbon number predominance (max at nC_{27}) to diminished odd-to-even predominance and increased dominance of low molecular weight *n*-alkane by Stage 3, reflecting progressive thermal evolution and maturation. The *n*-alkane in FS expelled oil showed a similar reduction in odd-to-even predominance but maintained a maximum molecular weight around nC_{17}–nC_{19} with no discernible shift (Fig. 8A).

A similar biomarker trend to that observed in bitumen is evident in the expelled oil of both HD and FS samples (Table 3). The CPI and OEP of expelled oil decreased progressively in both shales, with FS consistently exhibiting lower values than HD at equivalent stages. The Pr/Ph ratio of HD and FS samples initially increased from Stage 1 to Stage 2, but then decreased in Stage 3. The Pr/C_{17} and Ph/C_{18} ratios decreased continuously from Stage 1 to Stage 3, reflecting a decline in the relative abundance of pristane and phytane compared to their *n*-alkane homologues. Additionally, the Ts/(Ts + Tm) ratio decreased from Stage 1 to Stage 2 for both samples, suggesting an initial increase in maturity, but it increased at Stage 3, indicating that this biomarker maturity becomes unreliable as a maturity indicator at advanced stages due to the thermal destruction, consistent with the observation of C_{29} steranes behaviour in

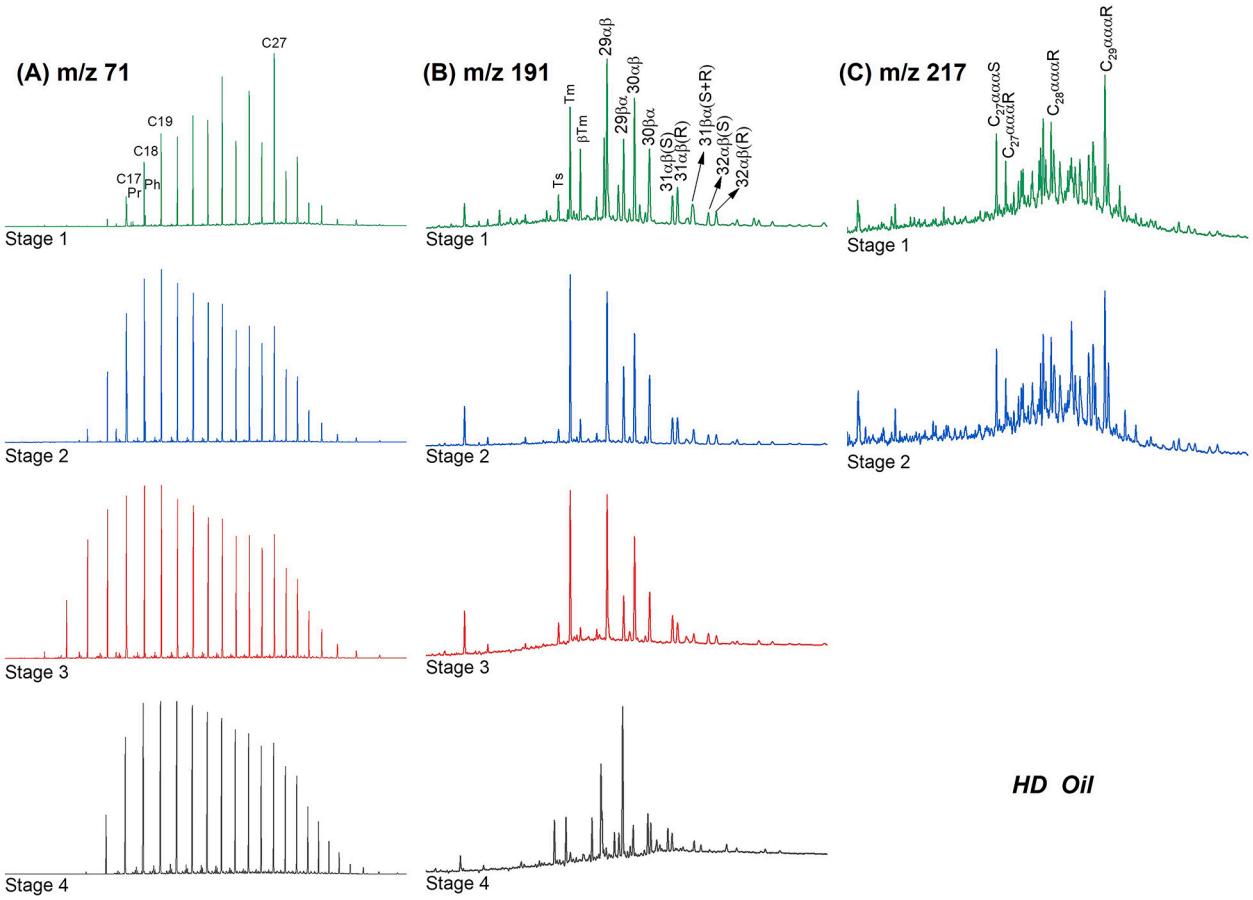

Fig. 7. Partial m/z 71, m/z 191, and m/z 217 mass chromatograms of the aliphatic hydrocarbon fraction in expelled oil from each stage of HD samples.

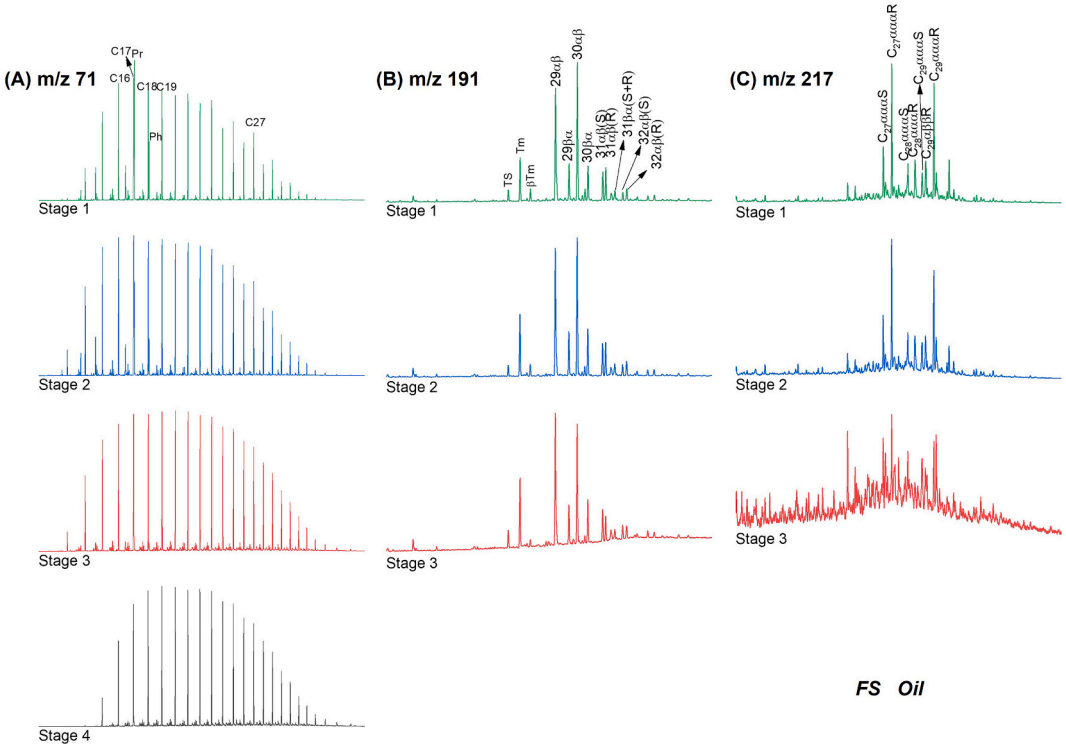

Fig. 8. Partial *m/z* 71, m/z 191, and m/z 217 mass chromatograms of the aliphatic hydrocarbon fraction in expelled oil from each stage of FS samples.

bitumen. As thermal evolution progressed from Stage 1 to Stage 3, the C_{29} βα/αβ and C_{30} βα/αβ ratios of HD oil decreased, while its C_{31} 22S/(22S + 22R) and C_{32} 22S/(22S + 22R) ratios increased. These changes suggest increasing maturity. In contrast, C_{29} βα/αβ and C_{30} βα/αβ ratios of FS oil fluctuated around 0.30 and 0.36, respectively, with only a slight increase observed in its C_{31} 22S/(22S + 22R) and C_{32} 22S/(22S + 22R) ratios. Additionally, the C_{29} ααα sterane 20S/(20S + 20R) ratio increased to 0.43 at Stage 2 of HD and to 0.54 at Stage 3 of FS. These biomarker trends collectively confirmed the progressive thermal maturation of expelled oils under experimental conditions for both shales.

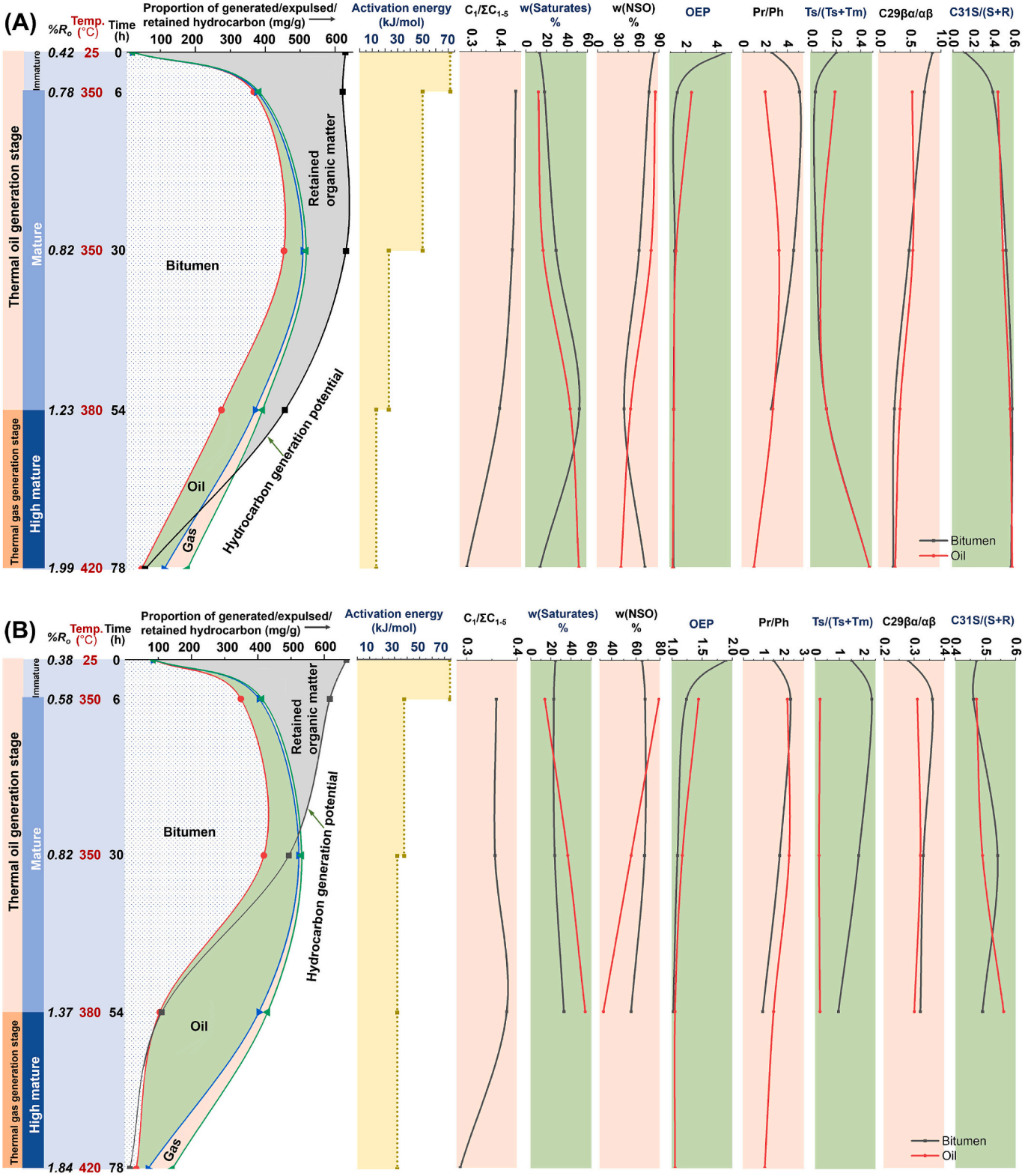

Fig. 9. Models of hydrocarbon generation, gas and oil expulsion, and retained bitumen during high-pressure hydrous pyrolysis: (A) HD shale and (B) FS shale.

3.2.4. Model of hydrocarbon generation

Fig. 9 presents hydrocarbon generation models for HD shale (Type II_1 kerogen) and FS shale (Type I kerogen), derived from the sequential high-pressure hydrous pyrolysis data. Activation energies (E_a) were calculated from thermogravimetric data using the Coats-Redfern kinetic model (10 °C min^{-1} heating rate; see Supplementary File). The organic matter enters an early maturity phase in Stage 1 (Phase I, Ro < 0.78 %), marked by the initiation of kerogen decomposition into abundant retained bitumen, with minimal oil and gas expulsion. Notably, both retained bitumen and expelled oil are dominated primarily by polar components, exhibiting low maturity levels. Both shales exhibit high initial E_a at this maturity phase, indicating that extensive decomposition of organic matter occurs during the process. This maturity window corresponds generally to the geochemical criteria for low-maturity shale oil, where hydrocarbon generation is in its incipient stage and bitumen retains characteristic low-maturity signatures.

As organic matter transformation progresses through the middle maturity stage in Stages 2 and 3 (Phase II, mature oil window), with mean Ro values ranging from 0.78 % to 1.23 %, the hydrocarbon-generation potentials declines gradually, accompanied by a decrease in E_a, indicating that less energy is required for kerogen conversion to bitumen and its subsequent decomposition compared to Phase I. For the FS shale, hydrocarbon-generation potential decreased from 411 mg/g to 97 mg/g in Stage 3, a reduction significantly greater than that observed for the HD shale. FS shale also underwent a distinct product shift, transitioning from bitumen to oil as the dominant generated hydrocarbon, with a higher proportion of aliphatic compounds in Stage 3 (Table S3). This reflects the inherent oil-proneness and advanced thermal reactivity of Type I kerogen under identical conditions. Meanwhile, this process was accompanied by greater energy requirements to crack complex bitumen molecules into lighter oil and gas compounds [43]; consequently, the E_a of FS shale decreased compared to the previous stage but remained higher in Stage 3, exceeding that of the HD sample. For HD shale, bitumen remained the primary product during this phase, accompanied by a simultaneous increase in oil and gas yields. Additionally, retained bitumen and expelled oil from Phase II exhibited a distinct decline in the odd-to-even predominance of *n*-alkane distribution, coupled with an increase in aliphatic proportions, indicating improved hydrocarbon maturity.

Upon reaching the late maturity to overmaturity phase (Phase III, Stage 4), the hydrocarbon-generation potential of organic matter is substantially depleted, accompanied by a decrease in bitumen and oil yields. Expelled gas yields increase significantly, driven by the secondary cracking of liquid hydrocarbons, as evidenced by declining dryness indices [35]. The E_a of HD further decreased in Phase III, whereas that of FS remained essentially unchanged. These differences in E_a evolution reflect distinct hydrocarbon generation pathways between HD and FS shale [44]. The overall reduction in E_a from Phase I to Phase III is associated with a continuous decrease in decomposable organic matter and lower energy requirements during thermal evolution. The relatively high E_a of FS in Phase III is due to the significant production of gaseous hydrocarbons via cracking of structurally complex organic compounds [43].

Compared to HD equivalents, FS residues and products consistently exhibit higher maturity levels of each stage. The divergent hydrocarbon generation pathways under high-pressure hydrous pyrolysis primarily stem from differences in geochemical properties. FS shale, dominated by Type I kerogen, possesses higher inherent oil propensity and reactivity than HD shale (Type II_1 kerogen), higher initial maturity and incorporates less terrestrial higher plant material. Furthermore, this confined high-pressure hydrous system facilitates bitumen formation as a major hydrocarbon product. As a critical intermediate in the kerogen-to-oil/gas transformation, bitumen persists in significant proportions before undergoing eventual cracking.

3.3. Implication for the in-situ conversion process of oil shale and low-maturity shale oil

The ISC process for oil shale and low-maturity shale oil, a complex physicochemical transformation, offers a promising pathway for mobilizing hydrocarbons from insoluble kerogen via subsurface heating. This technique facilitates the thermal decomposition of organic matter into producible oil and gas under geological conditions involving formation pressure and groundwater. Crucially, kerogen transformation occurs within a confined micro-rock environment, rendering our high-pressure (~500 bar) hydrous pyrolysis experiments, simulating depths relevant to low-maturity shale oil reservoirs (~5 km), highly informative for understanding ISC mechanisms.

Artificial thermal evolution enhances the organic matter maturity and hydrocarbon yield. The peak generation of mobilisable and oil-prone hydrocarbons occurs within a Ro range of 0.8–1.3 %, coinciding with a significant decline in residual hydrocarbon-generation potential. This delineates the optimal thermal maturity window for maximising liquid yield from oil shale and low-maturity shales during ISC operations. Beyond this peak oil window, secondary cracking of retained liquids, ongoing gas migration, and the generation of late-stage methane from refractory kerogen components continue to contribute to the hydrocarbon system.

Biomarkers in expelled oils provide reliable proxies and a non-destructive method for evaluating subsurface organic matter maturity, as evidenced by indicators such as decreasing OEP and CPI values and evolving sterane/hopane ratios. Coupled with declining gas dryness index ($C_1/\Sigma C_{1\text{-}5}$) at higher maturities, these parameters offer real-time, wellhead-monitorable indicators of thermal evolution progress during the ISC process, circumventing the impracticality of directly measuring Ro or T_{max} on deep subsurface residues.

It is evident that although the temperatures used in Stages 3 and 4 (380 °C and 420 °C respectively) were substantially lower than typical ex-situ retorting temperature (520 °C) [21,45], the hydrocarbon-generation potential underwent a marked decline during Stage 3, ultimately approaching zero after Stage 4, particularly for FS shale, signifying the completion of thermal evolution within the kerogen. This demonstrates the critical compensating role of heating duration. The prolonged heating inherent to ISC technology enables the effective pyrolysis of organic matter at relatively lower temperatures, enhancing energy efficiency and potentially reducing operational costs for immature and low-maturity resource development.

High in-situ pressure combined with the viscous nature of generated bitumen creates significant retention challenges that hinder hydrocarbon expulsion, a major hurdle for oil shale and low-maturity shale oil recovery. This underscores the necessity for engineered heating strategies (e.g., optimised heating rates, engineered fracture networks) to enhance fluid mobility and expulsion efficiency in low-permeability reservoirs. The distinct hydrocarbon generation trajectories of Type I (FS) versus Type II_1 (HD) kerogens, most notably FS's earlier transition to oil dominance, highlight the need for deposit-specific ISC process design. Oil shale or low-maturity shale oil plays with Type I kerogen may exhibit faster conversion kinetics and higher inherent oil potential under suitable thermal regimes.

While this study elucidates fundamental reaction pathways under geologically realistic pressures, direct extrapolation to field-scale production requires caution. Factors like heterogeneous heat distribution, reservoir heterogeneity, and fluid transport dynamics necessitate integration with reservoir simulations. Future pilot-scale ISC projects should correlate the geochemical characteristics of products (e.g., biomarkers, gas dryness index) with downhole maturity measurements and production logs, while establishing quantitative relationships between laboratory-derived E_a and field-scale energy input requirements. Additionally, predictive models integrating kerogen reactivity, pressure effects, and thermal stress duration should be developed to optimise ISC strategies for diverse organic-rich shale resources.

4. Conclusions

This study simulated the in-situ thermal evolution of immature HD (Type II_1 kerogen) and FS (Type I kerogen) shales under ~500 bar hydrostatic pressure via sequential hydrous pyrolysis.

The results showed that as artificial thermal pyrolysis proceeded, organic matter underwent sequential maturity progression, transitioning from the early maturity stage with bitumen-dominated composition (Stage 1, Ro < 0.78 %) through the peak oil generation phase with maximal liquid hydrocarbon yields (Stages 2–3, Ro = 0.78–1.23 %) to the late gas-prone maturity stage (Stage 4, Ro > 1.8 %). Concomitantly, hydrocarbon-generation potential declined systematically with thermal advancement. Type I kerogen (FS) exhibited higher inherent reactivity, generating more oil and gas at elevated maturity levels under identical conditions. Its earlier transition to oil dominance reflects inherent compositional advantages favorable for the ISC process. Biomarker evolution (e.g., OEP decline, sterane/hopane isomerization) in expelled oil and decreasing gas dryness index ($C_1/\Sigma C_1–C_5$) provide reliable proxies for subsurface maturation, circumventing the impracticality of solid-residue analysis (Ro, T_{max}) to infer the degree of thermal evolution and progress of the ISC process.

This work provides a mechanistic framework for kerogen transformation under conditions directly relevant to deep unconventional resource exploitation. High geological pressure impedes hydrocarbon mobility, necessitating engineered solutions for fluid recovery. The identified geochemical signatures offer practical tools for monitoring ISC progress, while the demonstrated efficacy of lower temperatures combined with prolonged heating informs the design of more efficient and economically viable thermal recovery strategies for these challenging resources.

CRediT authorship contribution statement

Fengtian Bai: Writing – original draft, Methodology, Investigation, Funding acquisition, Data curation. **Clement N. Uguna:** Writing – review & editing, Supervision, Methodology, Investigation, Conceptualization. **Will Meredith:** Writing – review & editing, Supervision. **Colin E. Snape:** Supervision, Funding acquisition. **Christopher H. Vane:** Writing – review & editing, Methodology. **Chenggong Sun:** Writing – review & editing, Supervision, Funding acquisition.

Declaration of competing interest

The authors declare that they have no known competing financial interests or personal relationships that could have appeared to influence the work reported in this paper.

Data availability

Data will be made available on request.

Acknowledgments

This work was supported by the National Natural Science Foundation of China (Grant No. 42202344), the Education Department of Jilin Province (Grant No. JJKH20250129KJ), the Science and Technology Department of Jilin Province (Grant No. 20250102102JC), and the Key Laboratory of Geophysical Exploration Equipment, Ministry of Education (Jilin University) (Grant No. GEIOF2023001).

Appendix A. Supplementary data

Supplementary data to this article can be found online at https://doi.org/10.1016/j.fuproc.2025.108327.

References

[1] R.C. Ryan, T.D. Fowler, G.L. Beer, V. Nair, Shell's In Situ Conversion Process–from Laboratory to Field Pilots. Oil Shale: A Solution to the Liquid Fuel Dilemma, ACS Publications, 2010, pp. 161–183.
[2] W.A. Symington, W.P. Kaminsky, W.P. Meurer, G.A. Otten, M.M. Thomas, J. D. Yeakel, ExxonMobil's electrofrac™ process for in situ oil shale conversion, ACS Symp. Ser. 1032 (2010) 185–216.
[3] Z. Kang, Y. Zhao, D. Yang, Review of oil shale in-situ conversion technology, Appl. Energy 269 (2020) 115121.
[4] Y. Sun, W. Guo, Q. Li, F. Bai, S. Deng, Current status and prospects of oil shale in-situ conversion technology in China, Petrol. Sci. Bullet. 8 (4) (2023) 475–490.
[5] W. Zhao, S. Hu, L. Hou, Connotation and strategic role of in-situ conversion processing of shale oil underground in the onshore China, Pet. Explor. Dev. 45 (4) (2018) 563–572.
[6] F.T. Bai, Y.H. Sun, Y.M. Liu, M.Y. Guo, J.M. Zhao, Characteristics and kinetics of huadian oil shale pyrolysis via non-isothermal thermogravimetric and gray relational analysis, Combust. Sci. Technol. 192 (3) (2020) 471–485.
[7] T. Liu, F. Liu, W. Shi, W. Li, B. Li, X. Liu, et al., Study on the kinetic-guided pyrolysis of oil shale kerogen catalyzed by needle-like NiFe-LDH, Fuel Process. Technol. 252 (2023) 107954.
[8] W. Zhao, S. Hu, L. Hou, T. Yang, X. Li, B. Guo, et al., Types and resource potential of continental shale oil in China and its boundary with tight oil, Petrol. Explorat. Develop. 47 (1) (2020) 1–11.
[9] W. Zhao, C. Bian, Y. Li, W. Liu, J. Dong, K. Wang, et al., Organic matter transformation ratio, hydrocarbon expulsion efficiency and shale oil enrichment type in Chang 73 shale of Upper Triassic Yanchang Formation in Ordos Basin, NW China, Petrol. Explorat. Develop. 50 (1) (2023) 14–26.
[10] X. Huang, Z. Kang, J. Zhao, G. Wang, H. Zhang, D. Yang, Experimental investigation on micro-fracture evolution and fracture permeability of oil shale heated by water vapor, Energy 277 (2023) 127677.
[11] S. Xu, Y. Sun, W. Guo, Q. Yang, Q. Li, M. Guo, et al., Regulating the oxidative assisted pyrolysis of Huadian oil shale by preheating temperature and oxygen flow rate, Energy 262 (2023) 125602.
[12] Q. Yang, W. Guo, S. Xu, C. Zhu, The autothermic pyrolysis in-situ conversion process for oil shale recovery: Effect of gas injection parameters, Energy (2023) 283.
[13] W. Qing, W. Xinmin, P. Shuo, Study on the structure, pyrolysis kinetics, gas release, reaction mechanism, and pathways of Fushun oil shale and kerogen in China, Fuel Process. Technol. 225 (2022) 107058.
[14] Z. Shuai, L. Xiaoshu, L. Qiang, S. Youhong, Thermal-fluid coupling analysis of oil shale pyrolysis and displacement by heat-carrying supercritical carbon dioxide, Chem. Eng. J. 394 (2020) 125037.
[15] X. Zhang, W. Guo, J. Pan, C. Zhu, S. Deng, In-situ pyrolysis of oil shale in pressured semi-closed system: Insights into products characteristics and pyrolysis mechanism, Energy 286 (2024) 129608.
[16] B. Baruah, P. Tiwari, Effect of high pressure on nonisothermal pyrolysis kinetics of oil shale and product yield, Energy Fuel 34 (12) (2020) 15855–15869.
[17] L. Su, D. Zhang, L. Zheng, X. Liu, X. Yang, J. Zheng, et al., Experimental study of the influences of pressure on generation and expulsion of hydrocarbons: a case study from mudstone source rocks and its geological application in the Tarim Basin, J. Petrol. Sci. Eng. 189 (2020) 107021.
[18] Z. Zhao, Q. Feng, X. Liu, H. Lu, Peng Pa, J. Liu, et al., Petroleum maturation processes simulated by high-pressure pyrolysis and kinetic modeling of low-maturity Type I kerogen, Energy Fuel 36 (4) (2022) 1882–1893.
[19] C.N. Uguna, A.D. Carr, C.E. Snape, W. Meredith, High pressure water pyrolysis of coal to evaluate the role of pressure on hydrocarbon generation and source rock maturation at high maturities under geological conditions, Org. Geochem. 78 (2015) 44–51.
[20] W. He, Y. Sun, X. Shan, Organic matter evolution in pyrolysis experiments of oil shale under high pressure: Guidance for in situ conversion of oil shale in the Songliao Basin, J. Anal. Appl. Pyrolysis 155 (2021) 105091.
[21] W. He, Y. Sun, W. Guo, X. Shan, Controlling the in-situ conversion process of oil shale via geochemical methods: a case study on the Fuyu oil shale, China, Fuel Process. Technol. 219 (2021) 106876.
[22] C.N. Uguna, A.D. Carr, C.E. Snape, W. Meredith, M. Castro-Díaz, A laboratory pyrolysis study to investigate the effect of water pressure on hydrocarbon generation and maturation of coals in geological basins, Org. Geochem. 52 (2012) 103–113.
[23] P. Whitelaw, C.N. Uguna, L.A. Stevens, W. Meredith, C.E. Snape, C.H. Vane, et al., Shale gas reserve evaluation by laboratory pyrolysis and gas holding capacity consistent with field data, Nat. Commun. 10 (1) (2019) 3654.
[24] C.N. Uguna, A.D. Carr, C.E. Snape, W. Meredith, I.C. Scotchman, A. Murray, et al., Impact of high water pressure on oil generation and maturation in Kimmeridge Clay and Monterey source rocks: Implications for petroleum retention and gas generation in shale gas systems, Mar. Pet. Geol. 73 (2016) 72–85.
[25] K.E. Peters, K.E. Peters, C.C. Walters, J. Moldowan, The Biomarker Guide, Cambridge University Press, 2005.
[26] L. Jiang, S.C. George, Biomarker signatures of Upper cretaceous Latrobe Group hydrocarbon source rocks, Gippsland Basin, Australia: distribution and palaeoenvironment significance of aliphatic hydrocarbons, Int. J. Coal Geol. 196 (2018) 29–42.
[27] E.S. Scalan, J.E. Smith, An improved measure of the odd-even predominance in the normal alkanes of sediment extracts and petroleum, Geochim. Cosmochim. Acta 34 (5) (1970) 611–620.

[28] K.E. Peters, J.M. Moldowan, The Biomarker Guide: Interpreting Molecular Fossils in Petroleum and Ancient Sediments, Englewood Cliffs Nj Prentice Hall, 1993.
[29] J. Tian, J. Liu, Z. Zhang, F. Cong, Hydrocarbon-generating potential, depositional environments, and organisms of the Middle Permian Tarlong Formation in the Turpan-Hami Basin, northwestern China, GSA Bull. 129 (9–10) (2017) 1252–1265.
[30] K.L. French, J.E. Birdwell, P.G. Lillis, Geochemistry of the cretaceous Mowry Shale in the Wind River Basin, Wyoming, GSA Bullet. 135 (7–8) (2022) 1899–1922.
[31] J.K. Volkman, S.M. Barrett, S.I. Blackburn, M.P. Mansour, E.L. Sikes, F. Gelin, Microalgal biomarkers: a review of recent research developments, Org. Geochem. 29 (5) (1998) 1163–1179.
[32] P.J. Grantham, L.L. Wakefield, Variations in the sterane carbon number distributions of marine source rock derived crude oils through geological time, Org. Geochem. 12 (1) (1988) 61–73.
[33] K.E. Peters, J.M. Moldowan, A.R. Driscole, G.J. Demaison, Origin of beatrice oil by co-sourcing from devonian and middle jurassic source rocks, Inner Moray Firth, United Kingdom, AAPG Bull. 73 (4) (1989) 454–471.
[34] M. Zhang, G. Huang, G. Hu, H. Zhao, Geochemical study on oil-cracked gases and kerogen-cracked gases (I)—Experimental simulation and products analysis, Sci. China Ser. D Earth Sci. 52 (1) (2009) 1–9.
[35] S. Yu, E. Li, H. Xu, W. Huang, L. Zeng, L. Jiang, et al., Incorporation of wet gases to kerogen in petroleum formation and evolution, Org. Geochem. 180 (2023) 104605.
[36] A.K. Burnham, J.E. Clarkson, M.F. Singleton, C.M. Wong, R.W. Crawford, Biological markers from Green River kerogen decomposition, Geochim. Cosmochim. Acta 46 (7) (1982) 1243–1251.
[37] M.P. Koopmans, W.I.C. Rijpstra, M.M. Klapwijk, J.W. de Leeuw, M.D. Lewan, J.S. S. Damsté, A thermal and chemical degradation approach to decipher pristane and phytane precursors in sedimentary organic matter, Org. Geochem. 30 (9) (1999) 1089–1104.
[38] Y. Tang, M. Stauffer, Formation of pristene, pristane and phytane: kinetic study by laboratory pyrolysis of Monterey source rock, Org. Geochem. 23 (5) (1995) 451–460.
[39] R.P. Philp, Fossil Fuel Biomarker, 1985.
[40] E. Kolaczkowska, N.E. Slougui, D.S. Watt, R.E. Maruca, J.M. Moldowan, Thermodynamic stability of various alkylated, dealkylated and rearranged 17α- and 17β-hopane isomers using molecular mechanics calculations, Org. Chem. 16 (4–6) (1990) 0–1038.
[41] T. Powell, D. McKirdy, Relationship between ratio of pristane to phytane, crude oil composition and geological environment in Australia, Nat. Phys. Sci. 243 (124) (1973) 37–39.
[42] C. Zhonghong, Z. Ming, J. Qiang, R. Yongjun, Distribution of sterane maturity parameters in a lacustrine basin and their control factors: a case study from the Dongying Sag, East China, Petrol. Sci. 8 (3) (2011) 290–301.
[43] L. He, Y. Ma, C. Yue, J. Wu, S. Li, Kinetic modeling of Kukersite oil shale pyrolysis with thermal bitumen as an intermediate, Fuel 279 (2020) 118371.
[44] Bai FT, Sun YH, Liu YM, Li Q, Guo MY. Thermal and kinetic characteristics of pyrolysis and combustion of three oil shales. Energ. Conver. Manage. 2015;97(0): 374–381.
[45] F. Yu, P. Sun, K.A. Zhao, L. Ma, X. Tian, Experimental constraints on the evolution of organic matter in oil shales during heating: Implications for enhanced in situ oil recovery from oil shales, Fuel 261 (2020) 116412.